applied sciences

MDPI

Article

Porosity Structure Offering Improved Biomechanical Stress Distribution and Enhanced Pain-Relieving Potential

Chia-Cheng Lin [1,2,3], Chia-Yu Wu [4,5], Mao-Suan Huang [6,7], Bai-Hung Huang [3,8,9], Hsin-Hua Chou [2,10], Keng-Liang Ou [6,11,12,13], Chung-Ming Liu [3,14], Fang-Tzu Pai [3,5], Han-Wei Huang [4,*] and Pei-Wen Peng [5,*]

1 Department of Dentistry, Shin Kong Wu Ho-Su Memorial Hospital, Taipei 111, Taiwan; jiajeng.lin@msa.hinet.net
2 School of Dentistry, College of Oral Medicine, Taipei Medical University, Taipei 110, Taiwan; hhchou@tmu.edu.tw
3 Biomedical Technology R&D Center, China Medical University Hospital, Taichung 404, Taiwan; babyfireh@gmail.com (B.-H.H.); liuc@mail.cmu.edu.tw (C.-M.L.); M249108004@tmu.edu.tw (F.-T.P.)
4 Division of Oral and Maxillofacial Surgery, Department of Dentistry, Taipei Medical University Hospital, Taipei 110, Taiwan; borgiawu@gmail.com
5 School of Dental Technology, College of Oral Medicine, Taipei Medical University, Taipei 110, Taiwan
6 Department of Dentistry, Taipei Medical University-Shuang Ho Hospital, New Taipei City 235, Taiwan; hms4837@tmu.edu.tw (M.-S.H.); klouyu@gmail.com (K.-L.O.)
7 School of Oral Hygiene, College of Oral Medicine, Taipei Medical University, Taipei 110, Taiwan
8 Implant Academy of Minimally Invasive Dentistry, Taipei 106, Taiwan
9 Asia Pacific Laser Institute, New Taipei City 220, Taiwan
10 Dental Department of Wan-Fang Hospital, Taipei Medical University, Taipei 116, Taiwan
11 Department of Oral Hygiene Care, Ching Kuo Institute of Management and Health, Keelung 203, Taiwan
12 Health Sciences University of Hokkaido, Hokkaido 061-0293, Japan
13 3D Global Biotech Inc. (Spin-off Company from Taipei Medical University), New Taipei City 221, Taiwan
14 School of Dentistry, College of Medicine, China Medical University, Taichung 404, Taiwan
* Correspondence: b202095036@tmu.edu.tw (H.-W.H); apon@tmu.edu.tw (P.-W.P.)

Received: 27 February 2020; Accepted: 21 April 2020; Published: 26 April 2020

check for updates

Abstract: In this study, we developed a three-dimensional (3D) human body model and a body sculpting clothing (BSC) which was fitted onto that body to simulate the biomechanical stress variations of the BSC with different porosity structures using the finite element method. The mechanical properties of the BSC with different porosity structures were also examined through the tensile testing. Analytical results indicated that the Von Mises stress of the BSC with a porosity structure of 10.28% varied from 0.076 MPa to 337.79 MPa. As compared with a porosity structure of 35.18%, the von Mises stress varied from 0.067 MPa to 207.30 MPa. The von Mises stress decreased as the porosity increasing. Based on the statistical analysis findings, we obtained a formula to predict the biomechanical relationships (von Mises stress and strain) between the human body and porosity of the BSC. Therefore, these findings could offer potential information in the modification of BSC for pain-relieving applications.

Keywords: finite element method; biomechanical properties; porosity; pain-relieving

1. Introduction

The textiles and fibers in biomedical development have grown rapidly for therapy applications in recent years [1,2]. The medical textile covers medical products and devices from wound dressings and bandages to high-tech applications including vascular implants, tissue engineering stents, and other medical textiles [3–5]. The structures of polymers determine their utilization in various domains, but the selection for subsequent employment is mainly determined by the chemical and physical properties of the polymers.

As previous studies reported that the body sculpting clothing (BSC) has some applications in clinical reports, for example, varicose veins mitigation [6–8], scar management [9], etc. While some of the latest studies [10–12] have also indicated there are a growing number of clinical applications of functional textile technology that benefit patients with pain relief. In order to deliver better therapy effects in a constant period, the thermal functional textile is required to closely fit with the body curve and contact the target skin position with large area and distribute the heat energy evenly in case any overheating occurs. Therefore, the fabric composition might play an important role in the functional clothing and BSC. In general, polyamide (nylon) is the most common in functional clothing applications because of its superior chemical and physical properties [13]. However, recently, some ways to detect the dynamic pressure of the fabrics have emerged [14–17], but less proving that the nylon could hold the stresses, or the nylon would not force extra stresses on the human body during the BSC functioning [18,19]. Therefore, it is necessary to build a biomechanical model to prove the materials' properties if they would be used on the human body in biomedical and pain-relieving applications.

There were three types of simulation models to describe the fabric mechanical model [20,21] including energy method, spring force method, and finite element method. Both the energy method and spring force method used particles to simulate the fabric's three-dimensional (3D) structure, but the finite element method used surfaces to simulate the fabric 3D structure. The energy method used the particle energy formula that could be described by the geometric relationships between the particles. Then, the particle energy formula could present the tension, compression, bending, and shearing stresses in the fabric 3D structure. The spring force method was used the spring to describe the particles relationships in 3D space. Use the linear spring-damper equation to simulate the fabric mechanical model. The finite element method cut the 3D fabric model into small pieces, and it was also used to analyze the structure's stresses distribution. It is an appropriate method to describe the static method, also the biomechanical model of polymers. Although it might take a lot of time to calculate the simulation result, the finite element method is an approximate, numerical method for solving continuing mechanical problems. Accordingly, this study developed a 3D human body model and a BSC which was fitted onto that body to simulate the biomechanical properties of the BSC with different porosity structures using finite element method.

2. Materials and Methods

2.1. Materials Preparation

The commercial nylon fabrics were obtained from Lolinya International Corporation (Taipei, Taiwan). The nylon fiber diameter was almost 20 μm, and these fibers were spun together as loop structure to knit as BSC with different porosity. The warp-knitted BSCs (thickness of 2 mm) were observed by Keyence VHX-2000 digital optical microscope (Taipei, Taiwan). Then, an image processing system (Buehler OmniMet 9.0, Lake Bluff, IL, USA) was employed to calculate the porosity of the warp-knitted BSCs [22]. Subsequently, the digital captured images were converted using Avizo 7.0 software (Thermo Fisher Scientific, Waltham, MA, USA). Afterward, the setting routine of Buehler OmniMet software was used to calculate the percentage of the red area in the capturing images, which also means the porosity of the warp-knitted BSCs. First, set the threshold B/W (0-124) to detect the porosity. However, some pores had poorly detected areas in them, so we filled holes to deal with this problem. Finally, the setting routine gave us the percent area of the pores in the warp-knitted BSCs as a whole (Figure 1). According to their own porosity, the warp-knitted BSCs are named as BSC-1, BSC-2, BSC-3, BSC-4, BSC-5, BSC-6, and BSC-7, respectively (Table 1).

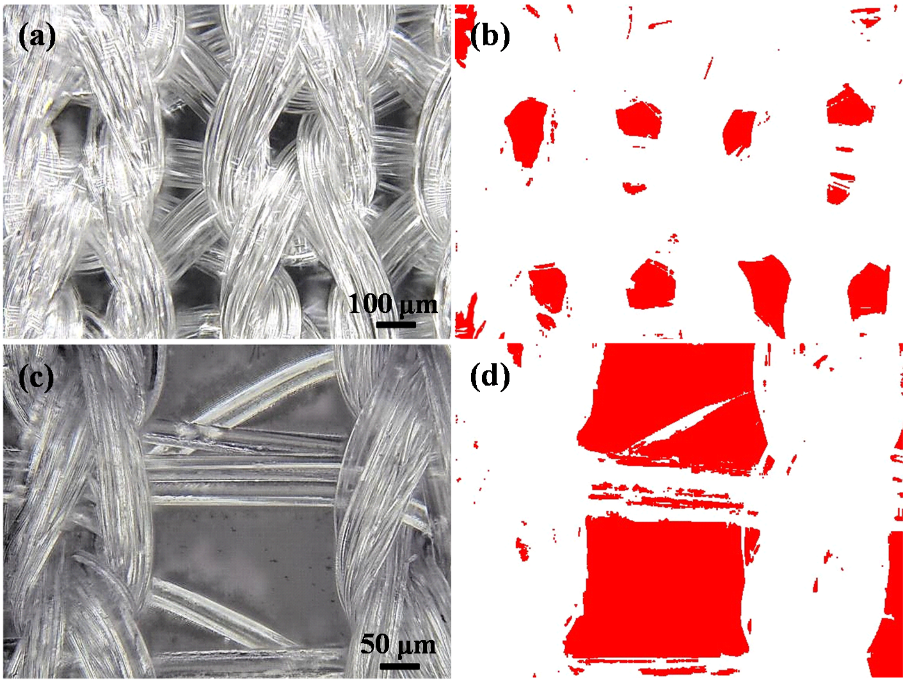

Figure 1. Image processing system: the capturing images and the threshold B/W: (**a**) BSC-1, (**b**) BSC-1 threshold B/W, (**c**) BSC-7, and (**d**) BSC-7 threshold B/W.

Table 1. Porosity of each warp-knitted BSC was calculated by the image processing system.

Samples	BSC-1	BSC-2	BSC-3	BSC-4	BSC-5	BSC-6	BSC-7
Porosity (%)	10.28	12.73	14.00	18.91	29.98	35.18	38.46

2.2. Fabrics Elastic Modulus Measurement

Mechanical properties were obtained via the LFPlus tensile machine (Taipei, Taiwan) with a loading of 1000 N, offering controlled uniformly loading force until sample maximum limitation of proportionality. The sample testing area was set as 1×3 cm. The elastic modulus of each sample could be determined. Use these elastic modules; we defined the material properties of the BSCs in later finite element analysis (FEA).

2.3. FEA Simulation

Based on the different elastic moduli between the different knitting densities, we tried to figure out how much stresses each sample caused on the human body during the decreasing abdomen circumference by FEA. The 3D human model and BSC model were built by Solidworks 2010 software (SolidWorks, Waltham, MA, USA) and combined together [23]. Then, the 3D models were built through the FEA software (ANSYS Workbench 12.1 version, Canonsburg, PA, USA). The human model takes a 176-cm woman as a basis, with a 29-inch waist circumference, 39-inch abdomen circumference and 41-inch buttocks circumference. The BSC model provided by Lolinya International Corporation and its specialty is abdomen-hugging to rebuild the body's golden ratio. In order to obtain a more accurate analysis, the 3D models' meshes were converted and reinforced (a tetrahedral element with 10 nodes was used for the mesh refinement) to make the FEA models reach to the real state and reliable. The mean numbers of nodes and elements are closed to 62,000 and 32,000, respectively (Figure 2). The mechanical properties of the BSCs were determined by the tensile testing, and the human model's biomechanical properties were defined as Table 2. Based on the desired abdomen circumference of 27 inches, the original waist circumference was 39 inch. The setting displacement 12 inch was applied on the abdomen portion of the BSC model. The boundary condition was fixed at the base of the human body model. Accordingly, no mutual movement between the human body model and BSC model at their interfaces was allowed. The material was assumed to be linear, isotropic, and homogeneous in the model assembly. Finally, the von Mises stress and stress distribution between the human body model and BSC model can be gained and compared in the study.

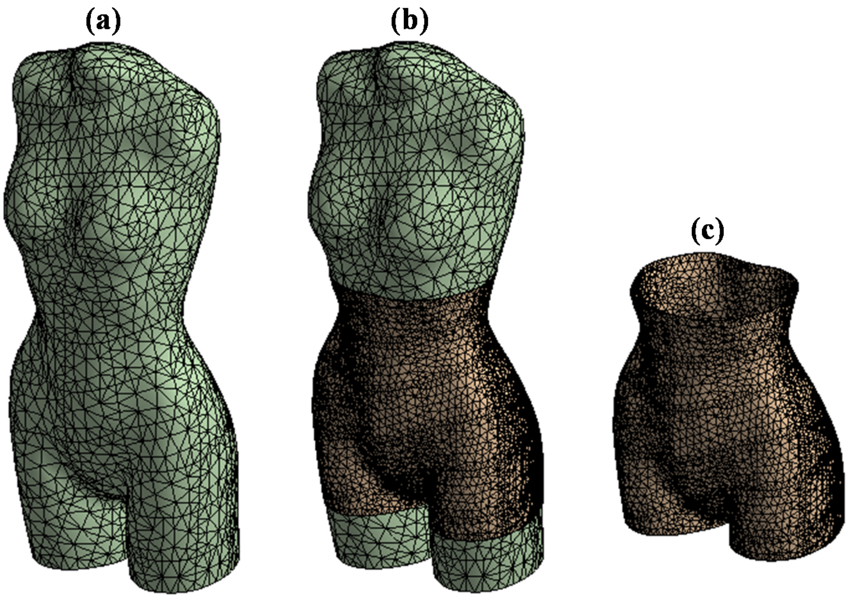

Figure 2. The 3D finite element meshed models. (**a**) The human body model, (**b**) the whole finite elements model, and (**c**) the BSC model.

Table 2. Mechanical properties of different materials of the model.

Materials	Elastic Modulus (MPa)	Poisson's Ratio
Human body	8.8×10^{-2}	0.22
Nylon	Determined by the tensile test	0.35

2.4. Statistical Analysis

The data were analyzed via the SPSS statistical software (IBM Statistics version 19, Armonk, NY, USA). Data were presented as mean ± standard deviation (p-value of <0.01 was considered significant). Pearson correlation coefficient as a statistical method in tensile testing was utilized to correlate the fabrics porosity parameters with the fabric's elastic modulus (multiple linear regression analysis). In finite element analysis, Pearson correlation coefficient used to correlate the fabrics porosity parameters with the von Mises stress of the human body.

3. Results and Discussion

3.1. Knitted Structure of the Nylon Fabric

The knitting porosity of the courses and wales knitting structure was observed using the digital optical microscope as shown in Figure 1. The nylon in the knitted BSC follows a tortuous path (a route), forming symmetrical loops above and below the average path of the nylon. These loops can be easily stretched in different directions, which can make BSC more elastic; depending on the bulk of the nylon, knitting patterns, and knitting porosity, the BSC can stretch as much as 500% [24,25]. Therefore, knitting was major using for the BSC that must be elastic or stretch in response to the human body movement [26,27]. Moreover, the courses and wales knitting structure are usually more form-fitting because their elasticity allows them to follow the human body's curvature closely. More extra curvature can be easily introduced into the fabrics without seams, such as the armpit portion, the crotch portion of the clothing can be harvested with short rows or by increasing or decreasing the number of stitches [28].

The image processing system was used to calculate the BSCs porosity, which is a reliable technique in measuring porosity [22], and the following porosity results were shown in Table 1. To determine the strength of the relationship between the porosity and the elastic modulus of the knitted BSCs, the data were analyzed in two sets and plotted against each other. By the correlation analysis, Pearson correlation coefficient is −0.898 ($p < 0.01$). In other words, the porosity and the elastic modulus of the knitted BSCs emerge a strong negative relationship. The linear correlation coefficient is $R^2 = 0.806$ ($p < 0.01$), and the linear regression Equation (1) and model (Figure 3) can be obtained.

$$E_{BSC} = E_{BSC}'(1 - 0.92P) \tag{1}$$

where P is porosity, E_{BSC} is the estimated average elastic modulus of the BSCs, and E_{BSC}' is the elastic modulus of the BSCs.

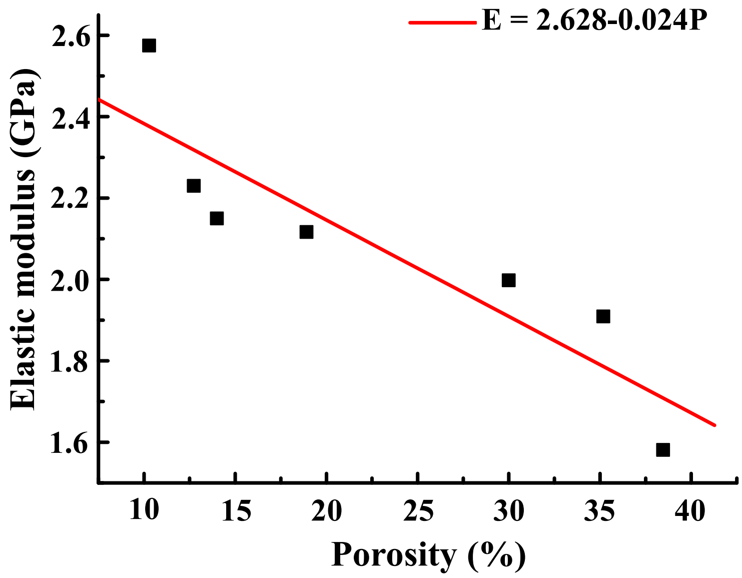

Figure 3. The linear regression model is the relationship between the porosity and the elastic modulus of the knitted BSCs.

3.2. Stress Transfer Behaviors

First, we wanted to investigate the relationship between the porosity of the knitted BSCs and the von Mises stresses of the human body during the BSC decreasing the model's abdomen circumference. Set the boundary conditions as the abdomen circumference decreasing 10 cm, and the following results as shown in Table 3. While the BSC-1 was used as the FEA model, the von Mises stresses were varied from 0.0076 MPa to 337.79 MPa (Figure 4), and most of stresses were concentrated in the crotch portion and the central abdomen portion. In the crotch portion, the BSC has less contact area with the human body. During the abdomen decreasing period, the clothing might cause more stress and pressure on the human body. Therefore, choosing the BSC in the crotch portion should be considered first, and we might choose a more soft and flexible BSC in the crotch portion of the clothing, or change the clothing design, such as the lock using, to prevent the stress concentration.

Table 3. Experiment results between the porosity, the elastic modulus of the knitted BSCs, the abdomen circumference decreasing, and the stress of the BSC and human body.

Porosity (%)	Elastic Modulus (GPa)	Stress of the BSC (MPa)	Stress of the Human Body (kPa)	Abdomen Circumference Decreasing (cm)
BSC-7 (38.46)	1.58	207.30	6.742	10
BSC-6 (35.18)	1.91	249.98	6.783	10
BSC-5 (29.98)	2.00	267.13	6.910	10
BSC-4 (18.91)	2.12	282.20	7.365	10
BSC-3 (14.00)	2.15	287.28	7.523	10
BSC-2 (12.73)	2.23	289.04	7.588	10
BSC-1 (10.28)	2.57	337.79	7.645	10
BSC-1 (10.28)	2.57	506.53	11.464	15
BSC-1 (10.28)	2.57	675.60	15.283	20
BSC-1 (10.28)	2.57	845.12	19.109	25
BSC-1 (10.28)	2.57	1032.48	22.825	30

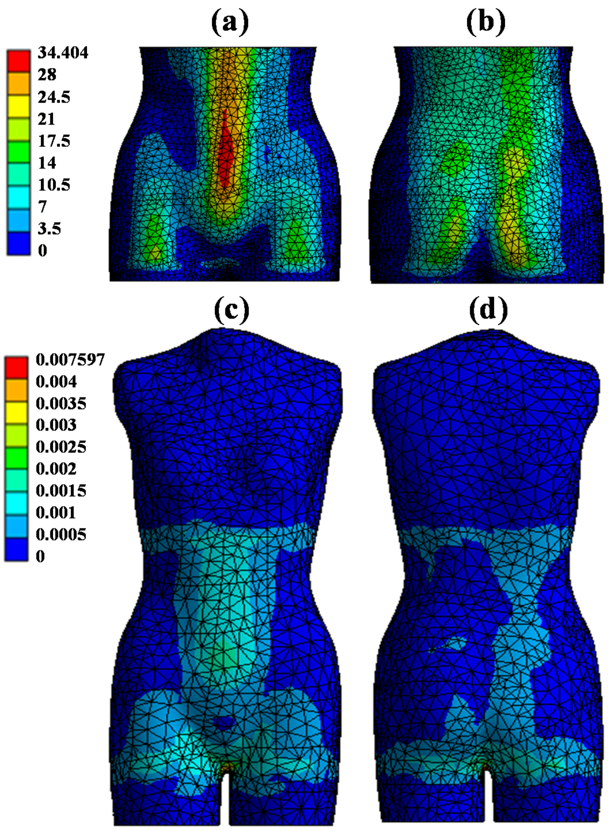

Figure 4. Von Mises stress distribution of the FEA results with BSC-1 sample during the abdomen decreasing period: (**a**) frontal view of the BSC, (**b**) back view of the BSC, (**c**) frontal view of the human body, and (**d**) back view of the human body.

After series FEA, the following results were calculated by SPSS. The von Mises stress of the human body was 7.22 ± 0.40 kPa. The relation between the porosity of the BSCs and the von Mises stress of the human body was calculated by the correlation analysis, Pearson correlation coefficient was −0.996 ($p < 0.01$). In other words, the porosity and the stresses on the human body emerge a strong negative relationship. The linear correlation coefficient is $R^2 = 0.991$ ($p < 0.01$), and the linear regression Equation (2) can be gained.

$$\sigma_{body} = \sigma_{body}'(1 - 0.43P) \tag{2}$$

where P is porosity, σ_{body} is the estimated stresses average of the human body, and $\sigma_{body}{}'$ is the stresses of the human body.

Then, increased the displacement of the abdomen circumference decreasing until the designed abdomen circumference 27 inch with BSC-1 sample. When the abdomen had decreased 12 inches (about 3-times the 10 cm displacement) (Figure 5), the von Mises stresses varied from 0.0228 MPa to 1032.5 MPa. As result, the following von Mises stresses of the BSC and the human body were growth in multiples with the displacement increased multiples. Therefore, we also used SPSS to conclude the Equation (3) which means the relationship between the porosity of the knitted BSCs (P), the displacement of the abdomen circumference decreasing (ΔL), the original length of the abdomen (L_0), the von Mises stresses of the human body ($\sigma_{body}{}'$) and the estimated von Mises stresses of the human body (σ_{body}). Thus, the linear correlation coefficient is $R^2 = 0.991$ ($p < 0.01$), and the linear regression Equation (3) and model (Figure 6) can be harvested.

$$\sigma_{body}(kPa) = \frac{\Delta L}{L_0}\left[\sigma_{body}{}'(7.37 - 3.17P)\right] \tag{3}$$

At the same time, the waist and buttocks circumference of the model would also be decreased, in which the waist circumference was decreased from 29 inch to 23 inch and the buttocks circumference was decreased from 41 inch to 34 inch. No matter how much the porosity of the knitted BSCs was, the same decreasing circumference results occurred.

It is well-known that functional clothing and BSC therapies are a convenient form of treatment used to revitalize the body and tender muscle tissue to bring about a reduction in muscle tension and offer pain-relief [10]. As mentioned above, it was found that there is significant difference in the relationship between the porosity of the BSCs and the stresses on the human body. The stress decreased as the porosity of BSC increasing. Hence, the stress level of the functional clothing or BSC could be adjusted to reduce the pressure of pain on the body. Currently, the latest issue on functional clothing with pain-relieving performance has been discussed using cannabidiol (CBD)-infused clothing. CBD is low tetrahydrocannabinol product derived from *Cannabis sativa* that has become very popular over the past few years. Patients report relief for a variety of conditions, particularly pain, without the intoxicating adverse effects of medical marijuana [29,30]. Much of the CBD is placed in strategic areas of the functional clothing so that it aligns with specific muscle groups. When wearing the clothes, the CBD releases through the dermal layer and into the pain point of the body. Accordingly, it would be desirable if the BCS could be combined with CBD without sacrificing desirable mechanical and biological properties for pain-relieving applications. Finally, more tests must be conducted to better understand the relationship between the pain-relieving property and BSCs with different porosities in the future.

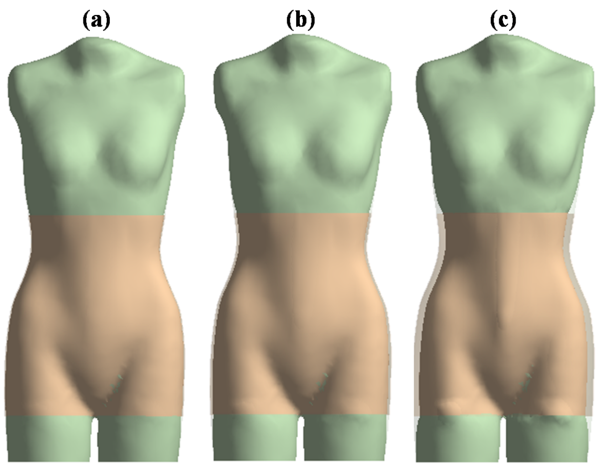

Figure 5. The human body deformed results while the abdomen circumference decrease was set as (**a**) 10 cm, (**b**) 15 cm, and (**c**) 30 cm.

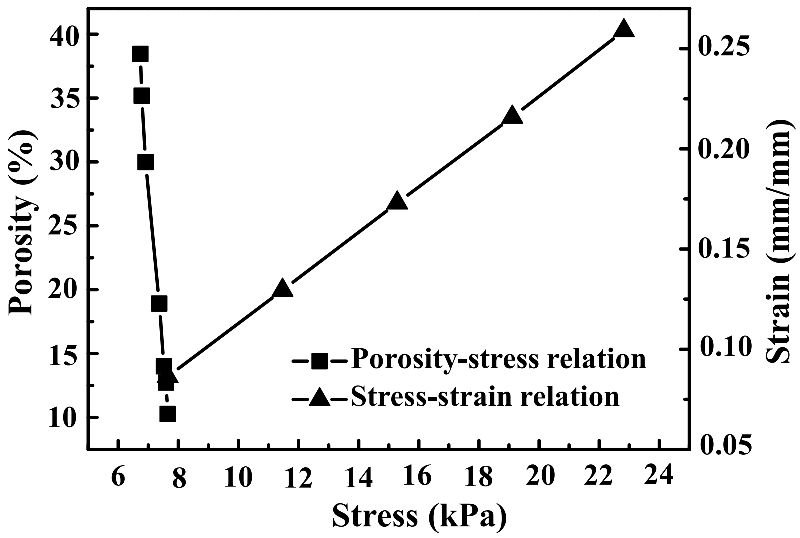

Figure 6. Regression model between the porosity of the fabrics, the strain, and the stress of the human body.

4. Conclusions

Through these investigations, first, we used an image processing system to analyze the porosity of the knitted BSCs and calculated the linear regression model. Then, we constructed a biomechanical model in BSCs by the FEA and found that there was significant difference in the relationship between the porosity of the BSCs and the stresses on the human body. Moreover, as the displacement increased in multiples, the stresses on the human body are grew in multiples. Therefore, the present data demonstrated a potential benefit in terms of providing biomechanical behaviors of the BSC for the human body.

Author Contributions: Writing—original draft, C.-C.L.; Investigation, C.-Y.W.; Data curation, B.-H.H. and F.-T.P.; Methodology, H.-H.C. and M.-S.H.; Validation, C.-M.L.; Supervision; K.-L.O.; Writing—review and editing, H.-W.H. and P.-W.P. All authors have read and agreed to the published version of the manuscript.

Funding: The authors would like to thank the Shin Kong Wu Ho-Su Memorial Hospital and Taipei Medical University for financially supporting this research under SKH-TMU joint research program contract no. SKH-TMU-104-06. This research was also supported in part by grant MOST 109-2622-8-038-005-TB1.

Conflicts of Interest: The authors declare no conflict of interest in this work.

References

1. Czajka, R. Development of medical textile market. *Fibres Text. East. Eur.* **2005**, *13*, 13–15.
2. Goswami, B.C.; Martindale, J.G.; Scardino, F. *Textile Yarns: Technology, Stracture, and Applications*; Wiley India Pvt Ltd.: Noida, India, 1977.
3. Dattilo, P.P., Jr.; King, M.W.; Cassill, N.L.; Leung, J.C. Medical textiles: Application of an absorbable barbed bi-directional surgical suture. *J. Text. Appar. Technol. Manag.* **2002**, *2*, 1–5.
4. King, M.W. Overview of opportunities in medical textiles. *Can. Text. J.* **2001**, *118*, 34–36.
5. Cooper, J.A.; Lu, H.H.; Ko, F.K.; Freeman, J.W.; Laurencin, C.T. Fiber-based tissue-engineered scaffold for ligament replacement: Design considerations and in vitro evaluation. *Biomaterials* **2005**, *26*, 1523–1532. [CrossRef] [PubMed]
6. Illouz, Y.-G. *Clinical Evaluation of Pressure Therapy in Conjunction with Aesthetic and Reconstructive Surgery*. 1989. Available online: https://www.medicalz.com/media/uploads/filemanager/plasticstudy.pdf (accessed on 12 January 2020).
7. Liu, R.; Kwok, Y.-L.; Li, Y.; Lao, T.-T. Fabric mechanical-surface properties of compression hosiery and their effects on skin pressure magnitudes when worn. *Fibres Text. East. Eur.* **2010**, *18*, 79.

8. Blattler, W.; Kreis, N.; Lun, B.; Winiger, J.; Amsler, F. Leg symptoms of healthy people and their treatment with compression hosiery. *Phlebology* **2008**, *23*, 214–221. [CrossRef]
9. Campbell, P.E.; Smith, G.S.; Smith, J.M. Retrospective clinical evaluation of gauze-based negative pressure wound therapy. *Int. Wound J.* **2008**, *5*, 280–286. [CrossRef]
10. Yang, C.; Li, L. The Application Wearable Thermal Textile Technology in Thermal-Protection Applications. *Trends Text. Fash Des.* **2018**, *1*, 22–30.
11. Yang, K.; Meadmore, K.; Freeman, C.; Grabham, N.; Hughes, A.M.; Wei, Y.; Torah, R.; Glanc-Gostkiewicz, M.; Beeby, S.; Tudor, J. Development of User-Friendly Wearable Electronic Textiles for Healthcare Applications. *Sensors* **2018**, *18*, 2410. [CrossRef]
12. Yang, K.; Isaia, B.; Brown, L.J.E.; Beeby, S. E-Textiles for Healthy Ageing. *Sensors* **2019**, *19*, 4463. [CrossRef]
13. Kojima, A.U.Y.; Masaya, K.; Akane, O.; Yoshiaki, F.; Toshio, K.; Osami, K. Mechanical properties of nylon 6-clay hybrid. *J. Mater. Res.* **1993**, *8*, 5. [CrossRef]
14. Wong, A.S.W.; Li, Y.; Zhang, X. Influence of fabric mechanical property on clothing dynamic pressure distribution and pressure comfort on tight-fit sportswear. *Sen-I Gakkaishi* **2004**, *60*, 293–299. [CrossRef]
15. Zhang, X.; Yeung, K.W.; Li, Y. Numerical simulation of 3D dynamic garment pressure. *Text Res. J.* **2002**, *72*, 245–252. [CrossRef]
16. Kang, T.J.; Kim, S.M. Optimized garment pattern generation based on three-dimensional anthropometric measurement. *Int. J. Cloth. Sci. Technol.* **2000**, *12*, 15.
17. Makabe, H.; Momota, H.; Mitsuno, T. A study of clothing pressure developed by the girdle. *J. Jpn. Res. Assoc. Text. End Uses* **1991**, *32*, 15.
18. Ohura, T.; Takahashi, M.; Ohura, N., Jr. Influence of external forces (pressure and shear force) on superficial layer and subcutis of porcine skin and effects of dressing materials: Are dressing materials beneficial for reducing pressure and shear force in tissues? *Wound Repair Regen* **2008**, *16*, 102–107. [CrossRef]
19. Li, Y.; Zhang, X.; Yeung, K.W. A 3D biomechanical model for numerical simulation of dynamic mechanical interactions of bra and breast during wear. *Sen-I Gakkaishi* **2003**, *59*, 12–21. [CrossRef]
20. House, D.; Breen, D. *Cloth Modeling and Animation*; A K Peters/CRC Press: Natick, MA, USA, 2000.
21. Matsuda, R.; Imaoka, H. A graphic method to simulate garment fitting on a human body model in various posture. *Sen'i Gakkaishi* **1995**, *51*, 9. [CrossRef]
22. Pourdeyhimi, B. Porosity of surgical mesh fabrics: New technology. *J. Biomed. Mater. Res.* **1989**, *23*, 145–152. [CrossRef]
23. Rodel, H. Relationship between knitting parameters, computer aided pattern design and fit of knitting underwear. *Int. J. Cloth. Sci. Technol.* **1999**, *11*, 2.
24. Chu, C.C.; Welch, L. Characterization of morphologic and mechanical properties of surgical mesh fabrics. *J. Biomed. Mater. Res.* **1985**, *19*, 903–916. [CrossRef] [PubMed]
25. Hiatt, J.H. *The Principles of Knitting: Methods and Techniques of Hand Knitting*; Simon & Schuster: New York, NY, USA, 1989.
26. Xie, S.T. Characterization of Interyarn Pore Size and its Distribution in Plain Woven Fabrics. Master's Thesis, North Carolina State University, Raleigh, NC, USA, 2002.
27. Karaguzel, B. Characterization and Role of Porosity in Knitted Fabrics. Master's Thesis, North Carolina State University, Raleigh, NC, USA, 2004.
28. Silvain, A.H. Form-Fitting Seamless Garment and Method. U.S. Patent 3,479,844, 25 November 1969.
29. VanDolah, H.J.; Bauer, B.A.; Mauck, K.F. Clinicians' Guide to Cannabidiol and Hemp Oils. *Mayo. Clin. Proc.* **2019**, *94*, 1840–1851. [CrossRef] [PubMed]
30. Baron, E.P. Comprehensive Review of Medicinal Marijuana, Cannabinoids, and Therapeutic Implications in Medicine and Headache: What a Long Strange Trip It's Been. *Headache* **2015**, *55*, 885–916. [CrossRef] [PubMed]